PHYSICAL REVIEW B **87**, 155301 (2013)

Subnanosecond magnetization dynamics induced by a pulsed magnetic field in diluted magnetic semiconductor quantum wells

Y. S. Chen,[1,*] M. Wiater,[2] G. Karczewski,[2] T. Wojtowicz,[2] and G. Bacher[1]

[1]*Werkstoffe der Elektrotechnik and CeNIDE, Universität Duisburg-Essen, Bismarckstr. 81, D-47057, Duisburg, Germany*

[2]*Institute of Physics, Polish Academy of Science, Al. Lotników32/46, 02-668, Warsaw, Poland*

(Received 3 December 2012; published 3 April 2013)

The magnetization dynamics induced by a pulsed magnetic field is investigated by time- and polarization-resolved photoluminescene measurements in (Cd,Mn)Te/(Cd,Mg)Te quantum wells. The magnetization dynamics of Mn^{2+} ions is found to be strongly dependent on the external static magnetic field. A dynamical response of the magnetization on a subnanosecond time scale is observed at zero static magnetic field, while it drastically slows down and approaches the spin-lattice relaxation time constant for a nonzero static field. Theoretical calculations emphasize the importance of local spin interactions that interplay with the Zeeman interaction for the observed magnetization dynamics.

DOI: 10.1103/PhysRevB.87.155301 PACS number(s): 75.78.−n, 78.47.jd, 78.55.Et

I. INTRODUCTION

To understand the spin dynamics of magnetic centers in semiconductors is fundamentally interesting as it indicates the potential rate of spin control in magnetically doped semiconductor spintronic devices.[1,2] The demonstration of electrically[3,4] and optically[4,5] controllable magnetism in diluted magnetic semiconductors (DMS) has stimulated vast investigations in order to evaluate the potential of this class of materials for spin-based applications.[6] Hereby, a critical issue is the question how fast magnetization can be controlled. Due to the isoelectronic configuration of localized Mn^{2+} ions and the absence of spin-orbit interaction (i.e., with zero orbit spin), the Mn^{2+} ions are widely treated as a model system of localized magnetic centers in II-Mn-VI semiconductors.[7–9] Most studies of Mn^{2+} ion spin dynamics are performed at a strong external static magnetic field (B_{ext}).[7,8] Nevertheless, as a significant prerequisite for spin-based information processing, the spin dynamic properties of Mn^{2+} ions especially at zero magnetic field are highly important, but hitherto rarely discussed in literature.[5,10–13]

Generally, the dynamic magnetization at a strong external magnetic field is regarded to be controlled by a spin lattice relaxation (SLR) process,[14] which involves an energy transfer via phonons between the spin system and the lattice system. Due to the weak coupling between Mn^{2+} ions and phonons, the SLR rate of Mn^{2+} ions in a DMS system is rather slow while it is found to be greatly enhanced by increasing the Mn content.[15–18] This is a result of the increased spin-spin interaction and the formation of Mn^{2+} ion clusters, in which fast SLR centers can relax the surrounding Mn^{2+} ions via spin diffusion.[17,19,20] In addition, carriers are demonstrated to accelerate the SLR process by opening the carrier-Mn^{2+} spin-flip channel.[21–23] Nevertheless, these effects cannot fasten the SLR process to less than 100 ns or below at the liquid helium temperature for a strong external magnetic field.[7,16] In case of zero magnetic field, however, spin relaxation has been found to be much faster than the inverse SLR rate.[11,13,15,16,24] This is ascribed to spin interactions with the local environment, either the Mn^{2+} ion spin-spin interaction[15,16,24] or the hyperfine interaction and the spin coupling with any local electric fields.[11] These local spin interactions can adiabatically induce fast state transitions, and thus bypass the slower SLR process.[11,16] Recently, it has been shown by Goryca *et al.*[11] that the rate of the magnetization dynamics can be varied by $3 \sim 4$ orders of magnitude by controlling B_{ext} and a fast magnetization dynamics beyond the SLR regime is observed with a time constant of ∼10 ns in the absence of an external magnetic field.

In this work, we study the magnetization dynamics induced by a pulsed magnetic field (B_{pul}) down to a few milliteslas by means of time- and polarization-resolved photoluminescence (PL) measurements in DMS quantum wells (QWs). An on-chip microcoil[25–27] is used to generate a fast magnetic field pulse with a transit time of ∼400 ps.[13] A magnetization dynamics on a subnanosecond time scale is observed in the absence of an external static field, while the time constants drastically slow down for a nonzero B_{ext} and approach values known for the SLR process. From Lindblad-type master equation simulations, the dependence of the magnetization dynamics on B_{ext} can be well understood as a result of the interplay between the Zeeman effect and the local spin interactions, i.e., hyperfine interaction, spin coupling with the cubic crystal field, local strain-induced electric field, and the spin-spin interaction between neighboring Mn^{2+} ions.

II. SAMPLES AND EXPERIMENTAL TECHNIQUE

The studied DMS samples were grown by molecular beam epitaxy on an undoped GaAs (001) substrate with a 2.47-μm-thick CdTe buffer layer. A DMS QW of $Cd_{1-x}Mn_xTe$ (sample 1: $x = 0.067$; sample 2: $x = 0.024$) with a thickness of 12 nm is embedded between a 1.23-μm-thick lower $Cd_{0.7}Mg_{0.3}Te$ barrier and a 70-nm $Cd_{0.7}Mg_{0.3}Te$ cap layer. Surface doping results in a hole density of $\sim 7 \times 10^{10}$ cm^{-2} in the QW.[28] Gold microcoils with a thickness of 350 nm are defined atop the semiconductor by electron-beam lithography and lift-off technique.[25–27] In Fig. 1(a), a typical microcoil with an aperture diameter of 8.5 μm and a width of 5.6 μm is shown. For such

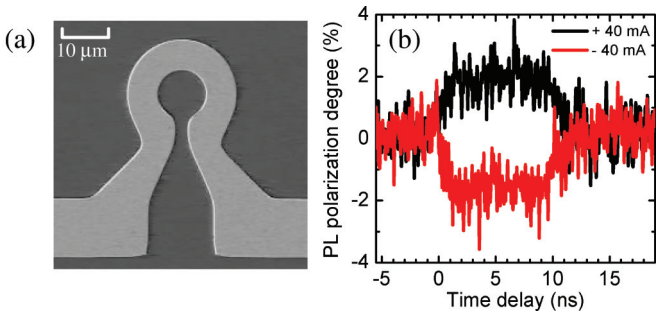

FIG. 1. (Color online) (a) Micrograph of a typical microcoil. The width is 5.6 μm and the inner aperture is 8.5 μm. (b) Time-resolved PL polarization induced by a pulsed current in sample 1 with $x_{Mn} = 0.067$. The pulse width is 10 ns, and the repetition period is 50 ns. The current is +40 mA for the black curve and −40 mA for the red one. The time delay t is with respect to the leading edge of the electric pulse.

a microcoil, a current-induced magnetic field of about 7.5 mT is generated in the microcoil center if the current amplitude is 100 mA.[25]

The pulsed field-induced magnetization dynamics was measured by the time- and polarization-resolved micro-PL spectroscopy. An additional static external field between −5 and 5 T could be applied in Faraday geometry, i.e., a magnetic field parallel to the light propagation direction. The sample was mounted in a cryostat on a helium flow-cooled copper finger that allows one to stabilize the sample temperature in the range from 3.7 to 300 K. The sample was excited with a cw linearly-polarized laser at the energy of 1.934 eV, which is above the DMS QW band gap but below the band gap of the barrier.[28] The laser was focused by a micro-objective with a N.A. = 0.75 and the spot diameter was less than 1 μm on the sample. The excitation power density was around 150 W/cm^2. The PL was modulated by an electro-optical modulator (EOM) and detected by a microchannel plate with a time resolution of 25 ps. The modulation phase was set at $+\pi/2$ and $-\pi/2$ for each half period (270 μs), and the EOM was synchronized with a time-correlated single photon counting (TCSPC) unit. By putting a linear polarizer at 45 degrees with respect to the EOM optical axes after the EOM, the right-circularly polarized (σ^+) and the left-circularly polarized (σ^-) PL intensity could be quasisimultaneously counted in the TCSPC unit. The whole cryostat system was adapted for 50 Ohm matching, and the sample was terminated by a 50-Ohm resistor. Two pulse generators have been applied to generate the voltage pulses: for a pulse sequence at a high repetition frequency (>15 MHz), a pulse generator (Agilent 81133A) with an edge transit time of 90 ps was used. Limited by the complex impedance of the metal microstructures and the cables inside the cryostat, a transit time of the voltage pulse through the microcoil of around 400 ps could be achieved.[13] In order to generate longer pulses, we used a second generator with a transit time of 2 ns (HP 8110A). The duty cycles of all the voltage pulse patterns used in this work have been fixed to 20%, and the sample temperature was 5 K for all the measurements.

III. EXPERIMENTAL RESULTS OF MAGNETIZATION DYNAMICS

In Fig. 1(b), typical time-resolved PL polarization measurements under the impact of a pulsed magnetic field are presented. The laser excitation is inside a microcoil with an aperture of 5 μm on sample 1. The magnetic field pulse duration is 10 ns and the current amplitude is 40 mA, which generates a magnetic field of $B_{pul} \approx 5$ mT in the microcoil center.[25] The Mn^{2+} ions are magnetized by B_{pul} and via the strong *sp-d* exchange interaction the optically excited carriers are strongly spin-polarized due to the giant Zeeman effect.[29] Since the carrier spin relaxation time is only a few picoseconds,[30] which is much shorter than the exciton lifetime of about 200 ps here, the dynamics of the PL polarization directly reflects the magnetization dynamics of the Mn^{2+} ions. The transient PL polarization at time t is given as $\rho(t) = [I^{\sigma+}(t) - I^{\sigma-}(t)]/[I^{\sigma+}(t) + I^{\sigma-}(t)]$, where the intensity of the σ^+-(σ^--) polarized PL is denoted by $I^{\sigma+}$ ($I^{\sigma-}$). Here, $t = 0$ defines the onset of the magnetic field pulse. For a positive current (black), a clear transient increase of $\rho(t)$ at the onset of the magnetic field pulse is observed, followed by saturation at about $\rho \sim 2.5\%$ and a rapid decay back to $\rho \sim 0$ after switching off the magnetic field. For the negative current (red), as expected, the polarization changes its sign, while the dynamics and the saturation magnitude of the polarization is virtually the same as in case of the positive current pulse. This fast polarization onset and decay indicates a much faster magnetization dynamics than recently reported by Goryca *et al.*, where time constants on the order of ∼10 ns have been obtained.[11]

The measured $\rho(t)$ is determined by the dynamic magnetization of the Mn^{2+} ions, written as $M(B_{tot}, T_{Mn}, t)$, and the exciton temperature $T_X(t)$. Here, $B_{tot}(t)$ is the amplitude of the total magnetic field, including the static external field and the pulsed field, i.e., $\boldsymbol{B}_{tot}(t) = \boldsymbol{B}_{ext} + \boldsymbol{B}_{pul}(t)$ and T_{Mn} is the effective spin temperature of the Mn^{2+} ions. In the regime of a low magnetic field, i.e., $B_{ext} \leqslant 100$ mT, the PL polarization can be approximated by a linear relation to the magnetization[25] as $\rho(t) \sim M(B_{tot}, T_{Mn}, t)\, T_X^{-1}(t)$. Also $M(B_{ext}, T_{Mn}, \Delta t) \sim B_{ext}\, T_{Mn}^{-1}(t)$ holds in the linear regime of the Brillouin function.[25] We now denote $\rho_+(t)$ as the dynamic PL polarization induced by a positive pulsed current with $B_{tot} = B_{ext} + B_{pul}$, and $\rho_-(t)$ for a negative one with $B_{tot} = B_{ext} - B_{pul}$. Since the dynamics of the spin temperature, $T_{Mn}(t)$, and the exciton temperature, $T_X(t)$, are expected to be independent on the current polarity, we define $\rho_{diff}(t) = 0.5[\rho_+(t) - \rho_-(t)]$, which is proportional to $M(B_{pul}, T_{Mn}, t)\, T_X^{-1}(t)$ and $\rho_{av}(t) = 0.5[\rho_+(t) + \rho_-(t)]$, which is proportional to $M(B_{ext}, T_{Mn}, t) \cdot T_X^{-1}(t)$. By comparing these two quantities, one can write $M(B_{pul}, T_{Mn}, t) = M(B_{ext}, T_{Mn}, t)\rho_{diff}(t)/\rho_{av}(t)$. As $T_{Mn}(t)$ can be assumed to be constant in the time regime under investigation,[25] we obtain

$$M(B_{pul}, T_{Mn}, t) \sim B_{ext} \cdot \rho_{diff}(t)/\rho_{av}(t). \quad (1)$$

This equation is used to evaluate the magnetization dynamics in the following. In this work, the averaged PL polarization $\rho_{av}(t)$ at $B_{ext} = 100$ mT is used to evaluate the spin temperature of the Mn^{2+} ions,[25] which is found to be about 10 K due to the current-generated heating for both samples. The quantity

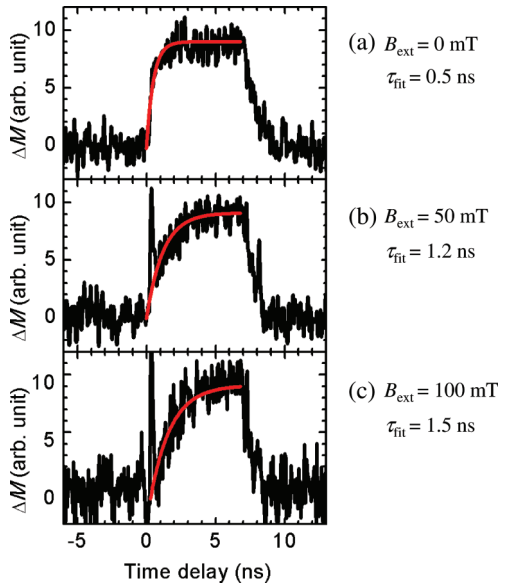

FIG. 2. (Color online) Magnetic field dependence of magnetization dynamics induced by a pulsed field for sample 1 with $x_{Mn} = 0.067$. The pulse width is 7 ns with a repetition period of 35 ns, and the current amplitude is 120 mA. The formation process is fitted exponentially with τ_{fit} (red lines). The time delay $t = 0$ represents the leading edge of the electric pulse. (a) External field $B_{ext} = 0$ mT and fitting constant $\tau_{fit} = 0.5$ ns; (b) $B_{ext} = 50$ mT and $\tau_{fit} = 1.2$ ns; (c) $B_{ext} = 100$ mT and $\tau_{fit} = 1.5$ ns.

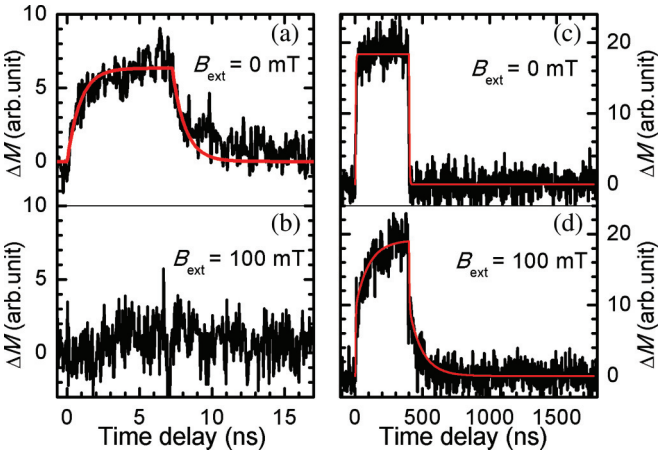

FIG. 3. (Color online) Magnetic field dependence of the magnetization dynamics induced by a pulsed field for sample 2 with $x_{Mn} = 0.024$. For (a) and (b), the current amplitude is 120 mA, and the pulse width is 7 ns with a repetition period of 35 ns. The time delay is with respect to the leading edge of the electric pulse. (a) External field $B_{ext} = 0$ mT; both the formation and the decay process (red lines) are exponentially fitted with a time constant of $\tau_{fit} = 0.9$ ns. (b) $B_{ext} = 100$ mT. For (c) and (d), the current amplitude is 200 mA, and the pulse width is 400 ns with a repetition period of 2 μs. (c) $B_{ext} = 0$ mT; both the formation and decay process (red lines) are exponentially fitted with a time constant $\tau_{fit} = 3$ ns. (d) $B_{ext} = 100$ mT. Both the formation and decay process (red lines) are biexponentially fitted by two time constants: $\tau_{fit1} = 3$ ns and $\tau_{fit2} = 100$ ns.

$\rho_{diff}(t)$ is obtained for different values of B_{ext}, i.e., 0, 50, and 100 mT, to investigate the magnetization dynamics at the corresponding B_{ext}.

In Figs. 2(a)–2(c), the pulse-induced magnetization dynamics is presented for different values of B_{ext} in sample 1 ($x_{Mn} = 0.067$). The pulse width is 7 ns, and the used microcoil is as presented in Fig. 1(a). The current amplitude is 120 mA generating $B_{pul} \approx 9$ mT. Since the repetition period of 35 ns is much shorter than the phonon lifetime,[25] the Mn^{2+} ion spins and the lattice system are in a thermal quasiequilibrium state. In case of $B_{ext} = 0$, the dynamics of the pulse-induced magnetization is clearly below 1 ns. It can be well fitted by an exponential law (red line) with a time constant of $\tau_{fit} = 0.5$ ns. Once an external field of 50 mT is applied, the formation process of the magnetization is obviously slowed down and it can be fitted with $\tau_{fit} = 1.2$ ns. The magnetization dynamics is further slowed down to $\tau_{fit} = 1.5$ ns when B_{ext} is increased to 100 mT. Such a dependence of the magnetization formation dynamics on the external magnetic field is also observed by using another microcoil on this sample. The trend that an external field can strongly slow down the magnetization dynamics is generally in a good agreement with the reported results by Goryca *et al.* for samples with an extremely low Mn-concentration x_{Mn} of $0.002 \leqslant x_{Mn} \leqslant 0.015$.[11] The spikes observed at time delay zero for a nonzero B_{ext} most likely originate from an electric field-induced transient carrier density in the semiconductor, which is different for a positive voltage pulse and a negative one. These transient carriers can change the magnetic susceptibility of the Mn^{2+} ions[8,22,23] and the carrier temperature. Thus the magnetization dynamics obtained by evaluating $\rho_{diff}(t)$ can show spikes in the presence of the electrically induced non-equilibrium carriers. The width of the spikes indeed correlates with the carrier lifetime of roughly 100 ps. As the density of these electrically induced nonequilibrium carriers—estimated from the transient PL intensity—is not sufficient to drastically change the spin relaxation rate of the Mn^{2+} ions,[8,22,23] these spikes do not affect the magnetization dynamics discussed in this work.

To further explore the B_{ext} dependence of the magnetization dynamics, similar measurements have been performed in sample 2 ($x_{Mn} = 0.024$). The evaluated magnetization dynamics is presented in Fig. 3. In Fig. 3(a), the data are plotted for $B_{ext} = 0$ mT and a fast magnetization dynamics is observed, where both the formation and the decay process can be fitted by $\tau_{fit} = 0.9$ ns. This is quite close to the case of sample 1, albeit the two Mn contents are quite different and the SLR rates are expected to differ by roughly two orders of magnitude.[16] In contrast, there is no pronounced magnetization formation within the pulse width of 7 ns once an external field of 100 mT is applied [see Fig. 3(b)]. This indicates a significantly enhanced magnetization time at $B_{ext} = 100$ mT for sample 2 as compared to sample 1.

This becomes much clearer if much longer current pulses are applied, as shown in Figs. 3(c) and 3(d). The pulse width is increased to 400 ns with an edge transit time of 2 ns, and B_{pul} is increased to ~20 mT. In the absence of B_{ext}, the magnetization dynamics is quasi-instantaneous on this time scale, as presented in Fig. 3(c): both the formation and the decay process are fitted by $\tau_{fit} = 3$ ns (red line), mainly limited by the enhanced transit time of the pulse generator as compared to the data shown in Figs. 3(a) and 3(b). Interestingly, as shown in Fig. 3(d), the magnetization

dynamics is slowed down once an external field of 100 mT is applied. Moreover, the magnetization dynamics, either the formation or the decay, is apparently composed of a fast process and a clearly slower one. Each process can be well fitted biexponentially with a short time constant of $\tau_{\text{fit1}} = 3$ ns and a longer one of $\tau_{\text{fit2}} = 100$ ns. The amplitude ratio of these two components is roughly 1:1. Such a biexponential spin dynamics is observed for different values of B_{pul} and pulse widths on this sample. These observations coincide well with the reported dynamics by Goryca *et al.*:[11] a pronounced slower magnetization dynamics appears once an external magnetic field is applied. Thereby the fast component can be suppressed if a strong magnetic field on the order of 1 T is applied.

The observed magnetization dynamics can be summarized as follows: (i) in the absence of B_{ext}, the spin dynamics is clearly on a subnanosecond time scale *independent* on the Mn content and (ii) an external field apparently slows down the spin dynamics and the slow process *depends* on the Mn content.

IV. NUMERICAL SIMULATIONS OF MAGNETIZATION DYNAMICS

In order to understand these findings, we consider in a first approximation the spin dynamics of isolated Mn^{2+} ions, neglecting the spin-spin interaction between neighboring Mn^{2+} ions. The Hamiltonian of a single isolated Mn^{2+} ion is given by[11]

$$\begin{aligned} H &= H_z + H_{\text{hf}} + H_{\text{cub}} + \sum H_{\text{strain}} + H_{\text{elec}}, \quad \text{with} \\ H_z &= g_{\text{Mn}}\mu_B \boldsymbol{B}_{\text{tot}} \cdot \boldsymbol{S}, \\ H_{\text{hf}} &= A\boldsymbol{I} \cdot \boldsymbol{S}, \\ H_{\text{cub}} &= \frac{a}{6}\left[S_x^4 + S_y^4 + S_z^4 - \frac{S(S+1)(3S^2+3S+1)}{5}\right], \\ H_{\text{strain}} &= D_s\left[S_z^2 - \frac{S(S+1)}{3}\right] + E_s\left[S_x^2 - S_y^2\right]. \end{aligned} \tag{2}$$

Hereby, $\boldsymbol{S}$ and $\boldsymbol{I}$ are the electron spin and the nuclear spin of the Mn ion, respectively. $\boldsymbol{B}_{\text{tot}}$ denotes the total external magnetic field, which defines the direction of the spin component S_z. The first term H_z is the Zeeman energy with the Mn^{2+} ion g factor of $g_{\text{Mn}} \approx 2.01$.[14] The second term H_{hf} is the hyperfine interaction with a hyperfine coupling constant $A \approx 0.68\ \mu$eV.[11] The spin coupling with the cubic crystal field is given in the third term H_{cub} with $a \approx 0.32\ \mu$eV.[11] The fourth term H_{strain} is the Mn ion spin coupling with a strain-induced electric field. In the studied (Cd, Mn)Te/$Cd_{0.7}Mg_{0.3}$Te DMS QW, the uniaxial strain along the growth direction (z axis) is around $\varepsilon_{zz} = -0.3\%$ by considering the mismatch of the crystal lattice constants.[31] The coefficients can be deduced as $D_s \approx 0.62\ \mu$eV and $E_s = 0$ for strain applied in [001] direction.[31–34] In case of an additional strain in [110] direction, both coefficients are nonzero. This can happen from local alloy fluctuations and dislocations. In Ref. 11, a strain of $\varepsilon_{xy} = 0.4\%$ is suggested for the (Cd,Mn)Te QWs, which gives $D_s \approx -0.41\ \mu$eV and $E_s = 0.40\ \mu$eV[31–35] as a lower-limit estimation for the investigated samples due to higher Mn contents. The last term H_{elec} describes the spin coupling with any electric field, which can be present due to the Fermi level pinning at the surface in the studied samples[28] or due to the applied voltage on the metal structures. The complete formalism is given in Ref. 36. Since the magnitude of the electric field is on the order of 10^7 V/m as an upper limit, H_{elec} is estimated to be only a few neV, and thus it can be neglected compared with the other terms.

Based on the spin Hamiltonian in Eq. (2), the magnetization dynamics of the Mn^{2+} ions can be phenomenally described by the Lindblad-type master equation:[37]

$$\frac{d\rho}{dt} = \frac{1}{i\hbar}[H, \rho_s] + (2L\rho_s L^+ - \{L^+L, \rho_s\}). \tag{3}$$

Here, H is the Mn^{2+} spin Hamiltonian, ρ_s is the spin density, L is the Lindblad operator, and $\hbar$ the reduced Planck constant. There are 36 states in the spin density matrix, i.e., $|S_i, I_j\rangle$ for the electron spin of S_i and the nuclear spin of I_j, as the electron spin and the nuclear spin of Mn^{2+} ions are both 5/2. The Lindblad operator can be simplified as $L = L_1 + L_2 + L_3$, with $L_1 = \Gamma_1\hat{\sigma}_+$, $L_2 = \Gamma_2\hat{\sigma}_-$, and $L_3 = \Gamma_3\hat{\sigma}_z$. The terms of L_1 and L_2 describe the spin-lattice relaxation process and the constants Γ_1 and Γ_2 are determined by the SLR rate and the Zeeman energy splitting between the spin subbands. Only the Mn^{2+} ion SLR is considered while the much longer nuclear SLR process is neglected.[38] The constant values are given by $\Gamma_1^{-1} = \tau_{\text{SLR}}(1 + e^{\Delta E/k_B T_{\text{Mn}}})$ and $\Gamma_2^{-1} = \Gamma_1^{-1}(1 + e^{-\Delta E/k_B T_{\text{Mn}}})$, where τ_{SLR} is the SLR time constant and ΔE is the energy splitting between the spin subbands. The term L_3 describes the spin-spin relaxation process and Γ_3 is here approximately the spin-spin relaxation rate. $\hat{\sigma}_+$, $\hat{\sigma}_-$, and $\hat{\sigma}_z$ are the Pauli matrices.

For the numerical simulations of the Mn^{2+} spin dynamics, the following parameters are used: $D_s = 0.62\ \mu$eV and $E_s = 0$ are used for the uniaxial strain, $D_s = -0.41\ \mu$eV and $E_s = 0.40\ \mu$eV for a [110] strain of 0.4%, and $D_s = -1.23\ \mu$eV and $E_s = 1.20\ \mu$eV for a [110] strain of 1.2%; the Mn^{2+} ion spin temperature for both samples is approximated by 10 K, a spin-spin relaxation time $\Gamma_3^{-1} = 500$ ps is assumed for both samples[16] and the SLR time is estimated to be $\tau_{\text{SLR1}} \approx 3$ ns at 10 K for sample 1 ($x = 0.067$) and $\tau_{\text{SLR2}} = 0.1\ \mu$s at 10 K for sample 2 ($x = 0.024$) by considering the reported low temperature SLR time constant[16] and the dependence of the SLR rate on temperature.[19] The magnetic pulse is assumed to be an ideal rectangular pulse, i.e., the edge transit time is zero, and the amplitude of the pulsed field is $B_{\text{pul}} = 9$ mT for sample 1 and $B_{\text{pul}} = 20$ mT for sample 2. As a result, the dynamic spin polarization of the Mn^{2+} ions is determined and the dynamic change relative to the spin polarization caused by the applied static field, i.e., $\Delta\rho_M(t)$, is calculated. As the magnetization $M(t)$ of the Mn^{2+} ions is linearly proportional to the spin polarization $\Delta\rho_M(t)$ of the Mn^{2+} ions, i.e., $M(t) = \Delta\rho_M(t) \cdot M_s$, with M_s as the saturation magnetization, the calculated dynamic spin polarization $\Delta\rho_M(t)$ directly represents the magnetization dynamics induced by the pulsed magnetic field.

In Figs. 4(a) and 4(b), the simulated magnetization dynamics of sample 1 and sample 2 are presented, respectively. The field dependence of the calculated magnetization dynamics is in a nice agreement with the experimental results: the formation and decay dynamics of the magnetization are both on a subnanosecond time scale (black solid lines) in case of zero field. Once an external field is applied, there are two different dynamic components, which can be nicely seen for sample 2 both in experiment and in the simulations. The

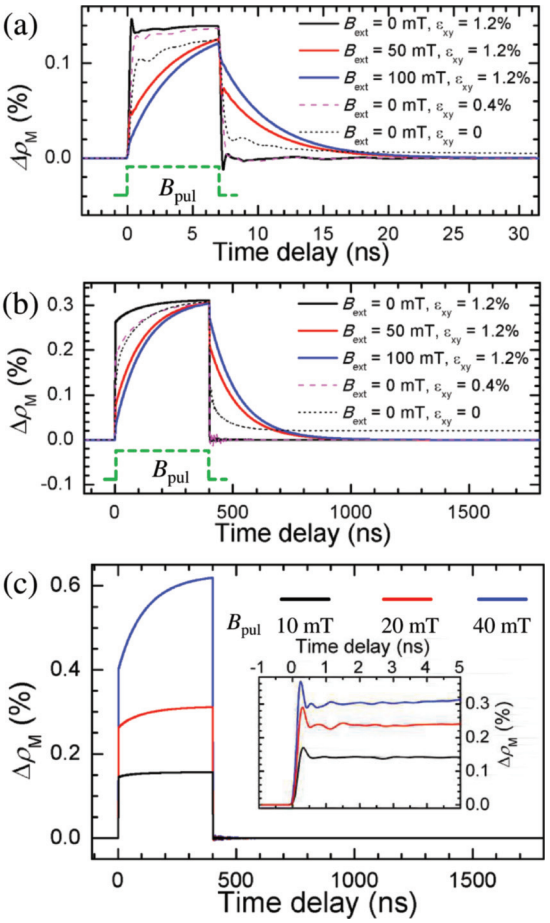

FIG. 4. (Color online) Numerically calculated magnetization dynamics of isolated Mn^{2+} ions induced by a pulsed magnetic field. The pulse is indicated by the green dashed line. Simulated magnetic field dependence of the magnetization dynamics for (a) sample 1 with $x_{Mn} = 0.067$ and (b) sample 2 with $x_{Mn} = 0.024$. Calculations are given for an external field of $B_{ext} = 0$ mT and an in-plane strain of $\varepsilon_{xy} = 1.2\%$ (black, solid line); for $B_{ext} = 50$ mT and $\varepsilon_{xy} = 1.2\%$ (red, solid line); for $B_{ext} = 100$ mT and $\varepsilon_{xy} = 1.2\%$ (blue, solid line); for $B_{ext} = 0$ mT and $\varepsilon_{xy} = 0$ (black, dashed line); for $B_{ext} = 0$ mT and $\varepsilon_{xy} = 0.4\%$ (magenta, dashed line). (c) Simulated pulsed field dependence of the magnetization dynamics in case of $B_{ext} = 0$ mT. The amplitude of the pulsed magnetic field is 10 (black), 20 (red), and 40 mT (blue). The inset presents the magnetization dynamics in the short time range with higher calculation accuracy.

fast component is thereby suppressed if the external magnetic field is increased to $B_{ext} = 50$ (red solid lines) and 100 mT (blue solid lines). The time constant of the slow component is close to the time constant assumed for the SLR process in the Lindblad-type master equation. Interestingly, if the local in-plane strain is not included ($\varepsilon_{xy} = 0$), there is a clearly observable slow component in both the spin onset and spin decay process even in case of zero B_{ext} (dashed black line), which is apparently absent in the experimental data shown in Fig. 3(c). This indicates that the strength of the well-known local spin interactions, e.g., hyperfine interaction and spin coupling with the crystal field and the uniaxial strain-induced electric field, is not large enough to completely surpass the slow component. This confirms the necessity of another spin interaction mechanism with off-diagonal elements, e.g., a possible local in-plane strain, to explain the uniform fast spin relaxation for different Mn contents in the absence of an external field. The origin of such a local in-plane strain is not clearly understood but might be related to dislocations and alloy or interface fluctuations. It has to be noted that the strength of each local spin interaction process, i.e., H_{hf}, H_{cub}, and H_{strain}, is rather similar, so each term contributes noticeably to the fast component.

Definitely any spin interactions resulting in an admixture of spin states can accelerate the magnetization dynamics bypassing the much slower SLR process. These local interactions break the orthogonality of the Zeeman interaction and can give rise to state anticrossings.[11] As a result, the stronger the local interaction is, the stronger magnetic field is required to suppress the state admixture. While switching the magnetic field pulse on and off, adiabatic state transitions happen at the energy levels of anticrossings, like many simultaneous Landau-Zener transitions.[11] The rate of these kinds of transitions is quite fast, and it is larger than $|H_{local}|/\hbar$ roughly by a factor of three if one considers the strength of state transitions for the large spin numbers,[39] i.e., $S = 5/2$ and $I = 5/2$. Hereby, $|H_{local}|$ is the strength of the total local spin interaction, and it is estimated as $|H_{local}| = |H_{hf}| + |H_{cub}| + |H_{strain}| \approx 3\,\mu$eV. This gives a state transition time <100 ps, which is much shorter than our time resolution and much shorter than the spin-spin relaxation time.

If the pulse amplitude is large, the pulse-induced magnetic field may become strong enough to separate the spin subbands by the Zeeman energy splitting, so that the energy levels of the spin states are too far away to generate state anticrossings. Then, the SLR process is expected to dominate the magnetization dynamics even in the absence of an external static field. This can be demonstrated by the calculated B_{pul} dependence of the magnetization dynamics as presented in Fig. 4(c) for sample 2. In case of $B_{pul} = 10$ mT (black line), the slow process is not clearly observable because the local interaction is stronger than the Zeeman interaction.[11] Increasing B_{pul} to 20 mT (red line), the slow process appears noticeably and the amplitude of the slow component becomes even comparable with the fast one for $B_{pul} = 40$ mT (blue line). Note that the saturation level of the Mn^{2+} ion spin polarization changes nearly linearly with the B_{pul} amplitude. The inset presents the simulated spin formation process on a shorter time scale, calculated with a much higher time resolution. Interestingly, the amplitude of the fast component is not linearly proportional to B_{pul}, even the magnetization is supposed to change linearly with the applied field in the weak field regime according to the Brillouin function. This can be reasonably understood by considering that the local spin interaction is the dominant factor that determines the amplitude and the transition rate of the fast component. Regarding the spin decay dynamics, there is no B_{pul} dependence. This is just as expected since the Zeeman effect vanishes and the spin dynamics is determined by the spin transitions at the anticrossings.

Now, we discuss possible effects from spin-spin interactions of the Mn^{2+} ions, i.e., beyond the model of isolated Mn^{2+} ions. There are three kinds of Mn^{2+} spin-spin interactions,[20] i.e., the Mn-Mn exchange interaction, the Dzyaloshinsky-Moriya (DM) interaction, and the dipole-dipole (DD)

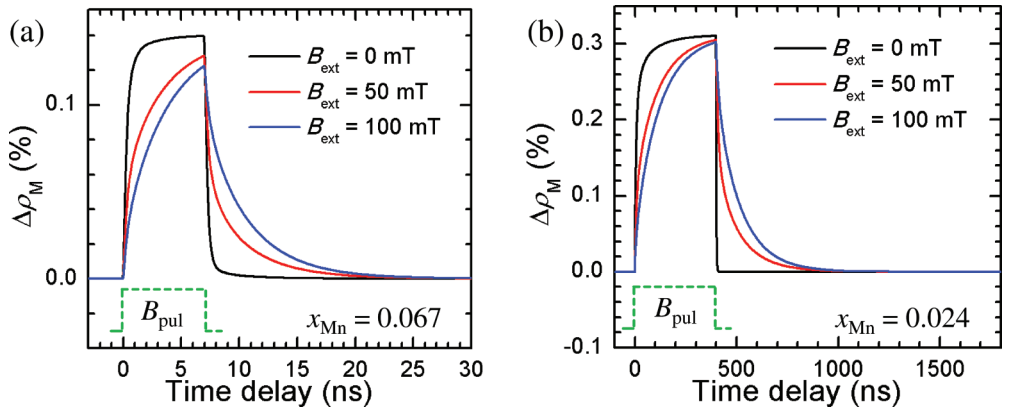

FIG. 5. (Color online) Numerically calculated magnetization dynamics of a coupled pair of Mn^{2+} ions induced by a pulsed magnetic field. The pulse is indicated by the green dashed line. Simulated magnetic field dependence of the magnetization dynamics for (a) sample 1 with $x_{Mn} = 0.067$ and $B_{pul} = 9$ mT; (b) sample 2 with $x_{Mn} = 0.024$ and $B_{pul} = 20$ mT.

interaction. The spin Hamiltonian of a coupled Mn-Mn pair is given as

$$\begin{aligned} H &= H_z + H_{ex} + H_{DM} + H_{DD}, \quad \text{with} \\ H_z &= g_{Mn}\mu_B \boldsymbol{B}_{tot} \cdot (\boldsymbol{S}_1 + \boldsymbol{S}_2), \\ H_{ex} &= -J \cdot (\boldsymbol{S}_1 \cdot \boldsymbol{S}_2), \\ H_{DM} &= -\boldsymbol{D} \cdot (\boldsymbol{S}_1 \times \boldsymbol{S}_2), \\ H_{DD} &= \frac{\mu_0 g_{Mn}^2 \mu_B^2}{4\pi} \left[\frac{\boldsymbol{S}_1 \cdot \boldsymbol{S}_2}{r_{12}^3} - \frac{3\,(\boldsymbol{S}_1 \cdot \boldsymbol{r}_{12}) \cdot (\boldsymbol{S}_2 \cdot \boldsymbol{r}_{12})}{r_{12}^5} \right]. \end{aligned} \tag{4}$$

Hereby $\boldsymbol{S}_1$ and $\boldsymbol{S}_2$ are the spin of Mn^{2+} ion 1 and Mn^{2+} ion 2, respectively. The first term is the Zeeman energy for two Mn^{2+} ions. The exchange interaction is described by H_{ex} and J is the coupling constant.[29] The third term is the DM interaction with $\boldsymbol{D}$ as the vector coefficient.[19] For the DD interaction, μ_0 is the vacuum permeability and $\boldsymbol{r}_{12}$ is the distance vector from Mn^{2+} ion 1 to Mn^{2+} ion 2.[14,38]

These spin-spin interactions can generate state admixture, and thus they can accelerate the spin dynamics, similar to the terms of the local spin interaction given in Eq. (2). The Mn-Mn exchange interaction is drastically dependent on the distance between two ions, and the strength is estimated to be less than 0.1 μeV for two Mn^{2+} ions located in different unit cells.[40] The DM interaction is always less than the exchange interaction.[19,41] Thus these two contributions are negligible for the fast magnetization dynamics of Mn^{2+} ions in different unit cells. In contrast, the DD interaction is long-distance ranged. The coupling strength is ~0.2 μeV (~0.07 μeV) as an upper (lower) estimate for two Mn^{2+} ions in neighboring unit cells.[14] Thus the DD contribution can be noticeable but still remains small compared with the hyperfine interaction (0.68 μeV) and the spin coupling with the crystal field (0.32 μeV) and the uniaxial strain (0.62 μeV).

On the other hand, the probability of finding a single Mn^{2+} ion in one face-center-cubic unit cell is roughly given by $(1-x_{Mn})$[12,42] which gives 44% for sample 1 and 75% for sample 2. This indicates there is a pronounced formation probability of Mn-Mn pairs or clusters in both samples. The spin diffusion between different unit cells cannot be the limiting factor of the subnanosecond magnetization dynamics, as the spin diffusion time between two nearest neighboring Mn^{2+} ions is estimated to be above the 10-ns time scale.[20] Taking a Mn-Mn pair within a same unit cell for instance, one finds the strength of the exchange interaction (DM interaction) can vary from a few 100 μeV (10 μeV) to less than 0.1 μeV (0.01 μeV) depending on the Mn-Mn distance, whereas the DD interaction strength is between ~0.2 and ~2 μeV. All three mechanisms can thus result in state anticrossings in the millitesla field regime. These spin-spin interactions can be noticeable especially for the sample of a higher Mn content, i.e., sample 1 with $x_{Mn} = 0.067$.

Based on the spin Hamiltonian in Eq. (4), the Lindblad-type master equation is applied to calculate the spin dynamics of a pair of coupled Mn^{2+} ions. For the simulations, we consider two Mn^{2+} ions diagonally located in one cubic face and displaced by $r_{12} = \sqrt{2}a_{Latt}$, in which a_{Latt} is the lattice constant. Here, the Mn-Mn exchange interaction constant is approximated as $J = -2.9$ μeV by considering its dependence on the Mn-Mn distance.[40] The DM interaction is neglected as its strength is estimated to be only ~5% of the Mn-Mn exchange interaction.[41] The DD interaction strength is determined to be ~0.35 μeV. For the Lindblad operators and the pulsed magnetic field for sample 1 and sample 2 the same values as for the calculations in Fig. 4 are used. The spin density matrix covers 36 states $|S_{1i}, S_{2i}\rangle$, in which S_{1i} and S_{2i} denote the spin states of two Mn^{2+} ions, respectively. The spin states of both Mn^{2+} ions are calculated, and the dynamic spin polarization based on two Mn^{2+} ions is determined.

The calculated dynamic spin polarization $\Delta\rho_M(t)$ is plotted in Figs. 5(a) and 5(b) for sample 1 and sample 2, respectively. For both samples, there is a fast spin onset and a spin decay in the absence of an external field, while the spin dynamics is clearly slowed down and close to the SLR regime if the static external field B_{ext} is increased. This behavior is qualitatively similar to the calculations presented in Figs. 4(a) and 4(b). In addition, the calculated saturation value of the spin polarization for a coupled Mn-pair is nearly the same as for isolated Mn ions, where the hyperfine interaction and the spin coupling with the local electric field are considered. That is, the saturation levels of the spin polarization are ~0.14% in both Figs. 4(a) and 5(a), and they are both ~0.3% in Figs. 4(b) and 5(b).

This indicates that besides hyperfine interaction and local electric fields also the Mn-Mn interaction can contribute to the experimentally observed fast magnetization dynamics for zero external field especially for a higher Mn content.

V. CONCLUSION

In conclusion, the magnetization dynamics of localized Mn^{2+} ions induced by a pulsed magnetic field is investigated by time- and polarization-resolved photoluminescence measurements in DMS QWs. A subnanosecond magnetization dynamics is observed independent of the Mn content in the absence of an external field, while the dynamics is clearly slowed down and becomes biexponential once a static magnetic field is applied. Theoretical calculations based on a Lindblad-type master equation demonstrate that the observed magnetization dynamics can be understood as an interplay between the Zeeman effect and the local spin interactions, i.e., hyperfine interaction, spin coupling with the crystal field, strain-induced field, and Mn-Mn interaction. These local spin interactions result in anticrossings of the Mn^{2+} spin states in the field regime of about 10 mT. This allows for fast adiabatic state transitions if the pulsed magnetic field is switched on or off. For a sufficiently strong external magnetic field, the Zeeman energy splitting between the spin states can suppress the adiabatic spin transitions, and thus the spin lattice relaxation process becomes dominant for the observed spin dynamics.

ACKNOWLEDGMENTS

The authors would like to thank M. Goryca for simulation discussions, H. Watzel for technical assistance, J. Puls, S. Otto, and X.D. Cui for useful suggestions concerning the high-frequency operation, and G. Salis for helpful discussions and suggestions. The work in Duisburg was financially supported by the Deutsche Forschungsgemeinschaft within the priority program SPP 1285 "Semiconductor spintronics." The research in Poland was partially supported by the European Union within European Regional Development Fund, through grant Innovative Economy (POIG.01.01.02-00-008/08).

*Electronic mail address to whom correspondence should be sent: ych@zurich.ibm.com. Current address: IBM Zurich Research Lab, Rüschlikon, CH-8803, Switzerland.

[1] D. D. Awschalom, D. Loss, and N. Samarth, *Semiconductor Spintronics and Quantum Computation* (Springer-Verlag, Berlin, 2002).

[2] J. Kossut, and J. A. Gaj, *Introduction to the Physics of Diluted Magnetic Semiconductors* (Springer, 2010), Vol. 144.

[3] H. Ohno, D. Chiba, F. Matsukura, T. Omiya, E. Abe, T. Dietl, Y. Ohno, and K. Ohtani, Nature (London) **408**, 944 (2000).

[4] H. Boukari, P. Kossacki, M. Bertolini, D. Ferrand, J. Cibert, S. Tatarenko, A. Wasiela, J. A. Gaj, and T. Dietl, Phys. Rev. Lett. **88**, 207204 (2002).

[5] R. Beaulac, L. Schneider, P. I. Archer, G. Bacher, and D. R. Gamelin, Science **325**, 973 (2009).

[6] T. Dietl, D. D. Awaschalom, M. Kaminska, and H. Ohno, *Spintronics* (Elsevier, 2008), Vol. 82.

[7] D. R. Yakovlev and I. A. Merkulov, in *Introduction to the Physics of Diluted Magnetic Semiconductors*, edited by J. Kossut and J. A. Gaj (Springer, 2010), pp. 253.

[8] A. V. Akimov, A. V. Scherbakov, and D. R. Yakovlev, in *Handbook of Semiconductor Nanostructures and Nanodevices*, edited by A. A. Balandin and K. L. Wang (American Scientific Publishers, 2006).

[9] L. Besombes, Y. Leger, L. Maingault, D. Ferrand, H. Mariette, and J. Cibert, Phys. Rev. Lett. **93**, 207403 (2004).

[10] J. Seufert, G. Bacher, M. Scheibner, A. Forchel, S. Lee, M. Dobrowolska, and J. K. Furdyna, Phys. Rev. Lett. **88**, 027402 (2001).

[11] M. Goryca, D. Ferrand, P. Kossacki, M. Nawrocki, W. Pacuski, W. Maślana, J. A. Gaj, S. Tatarenko, J. Cibert, T. Wojtowicz, and G. Karczewski, Phys. Rev. Lett. **102**, 046408 (2009).

[12] C. Le Gall, L. Besombes, H. Boukari, R. Kolodka, J. Cibert, and H. Mariette, Phys. Rev. Lett. **102**, 127402 (2009).

[13] Y. S. Chen, M. Wiater, G. Karczewski, T. Wojtowicz, and G. Bacher, Phys. Status Solidi B **247**, 1505 (2010).

[14] A. Abragam and B. Bleaney, *Electronic Paramagnetic Resonance of Transition Ions* (Clarendon, Oxford, 1970).

[15] D. Scalbert, J. Cernogora, and C. B. A. L. Guillaume, Solid State Commun. **66**, 571 (1988).

[16] T. Dietl, P. Peyla, W. Grieshaber, and Y. Merle d'Aubigné, Phys. Rev. Lett. **74**, 474 (1995).

[17] T. Strutz, A. M. Witowski, and P. Wyder, Phys. Rev. Lett. **68**, 3912 (1992).

[18] M. K. Kneip, D. R. Yakovlev, M. Bayer, A. A. Maksimov, I. I. Tartakovskii, D. Keller, W. Ossau, L. W. Molenkamp, and A. Waag, Phys. Rev. B **73**, 045305 (2006).

[19] D. Scalbert, Phys. Status Solidi B **193**, 189 (1996).

[20] A. A. Maksimov, D. R. Yakovlev, J. Debus, I. I. Tartakovskii, A. Waag, G. Karczewski, T. Wojtowicz, J. Kossut, and M. Bayer, Phys. Rev. B **82**, 035211 (2010).

[21] B. König, I. A. Merkulov, D. R. Yakovlev, W. Ossau, S. M. Ryabchenko, M. Kutrowski, T. Wojtowicz, G. Karczewski, and J. Kossut, Phys. Rev. B **61**, 16870 (2000).

[22] A. V. Scherbakov, D. R. Yakovlev, A. V. Akimov, I. A. Merkulov, B. König, W. Ossau, L. W. Molenkamp, T. Wojtowicz, G. Karczewski, G. Cywinski, and J. Kossut, Phys. Rev. B **64**, 155205 (2001).

[23] A. V. Scherbakov, A. V. Akimov, D. R. Yakovlev, W. Ossau, L. W. Molenkamp, S. Tatarenko, and J. Cibert, Solid State Commun. **120**, 17 (2001).

[24] M. A. Butler, S. J. Martin, and R. J. Baughman, Appl. Phys. Lett. **49**, 1053 (1986).

[25] Y. S. Chen, S. Halm, E. Neshataeva, T. Kümmell, G. Bacher, M. Wiater, T. Wojtowicz, and G. Karczewski, Appl. Phys. Lett. **93**, 141902 (2008).

[26] Y. S. Chen, D. Reuter, A. D. Wieck, and G. Bacher, Phys. Rev. Lett. **107**, 167601 (2011).

[27]Y. S. Chen, J. Huang, D. Reuter, A. Ludwig, A. D. Wieck, and G. Bacher, Appl. Phys. Lett. **98**, 081911 (2011).
[28]W. Maślana, P. Kossacki, M. Bertolini, H. Boukari, D. Ferrand, S. Tatarenko, J. Cibert, and J. A. Gaj, Appl. Phys. Lett. **82**, 1875 (2003).
[29]J. K. Furdyna, J. Appl. Phys. **64**, R29 (1988).
[30]M. R. Freeman, D. D. Awschalom, J. M. Hong, and L. L. Chang, Phys. Rev. Lett. **64**, 2430 (1990).
[31]O. Madelung, *Semiconductors: Data Handbook* (Springer, Berlin, 2004).
[32]M. Qazzaz, G. Yang, S. H. Xin, L. Montes, H. Luo, and J. K. Furdyna, Solid State Commun. **96**, 405 (1995).
[33]E. R. Feher, Phys. Rev. **136**, A145 (1964).
[34]M. T. Causa, M. Tovar, S. B. Oseroff, R. Calvo, and W. Giriat, Phys. Lett. A **77**, 473 (1980).
[35]E. Deligoz, K. Colakoglu, Y. Ciftci, Physica B **373**, 124 (2006).
[36]A. Kiel and W. B. Mims, Phys. Rev. B **5**, 803 (1972).
[37]H.-P. Breuer and F. Petruccione, *The Theory of Open Quantum Systems* (Oxford University Press, 2007).
[38]A. Abragam, *The Principles of Nuclear Magnetism* (Oxford University Press, Oxford, 1961).
[39]M. D. Fayer, *Elements of Quantum Mechanics* (Oxford University Press, Inc., New York, 2001).
[40]B. E. Larson, K. C. Hass, H. Ehrenreich, and A. E. Carlsson, Phys. Rev. B **37**, 4137 (1988).
[41]B. E. Larson and H. Ehrenreich, Phys. Rev. B **39**, 1747 (1989).
[42]M. M. Kreitman and D. L. Barnett, J. Chem. Phys. **43**, 364 (1965).